

Article

Failure Analysis and Reliability of Ni–Ti-Based Dental Rotary Files Subjected to Cyclic Fatigue

Abdullah Alqedairi ^{1,*} , Hussam Alfawaz ¹, Amani bin Rabba ¹, Areej Almutairi ¹, Sarah Alnafaiy ¹ and Muneer Khan Mohammed ²

¹ Department of Restorative Dental Sciences, College of Dentistry, King Saud University, P.O. Box 60169, Riyadh 11545, Saudi Arabia; halfawaz1@ksu.edu.sa (H.A.); dr.amoon@hotmail.com (A.b.R.); tootah1410@hotmail.com (A.A.); saranafaiy@yahoo.com (S.A.)

² Princess Fatima Alnijris's Research Chair for Advanced Manufacturing Technology, Advanced Manufacturing Institute, King Saud University, P.O. Box 800, Riyadh 11421, Saudi Arabia; muneer0649@gmail.com

* Correspondence: aalqedairi@ksu.edu.sa; Tel.: +966-114-677-420

Received: 12 November 2017; Accepted: 3 January 2018; Published: 6 January 2018

Abstract: The cyclic fatigue resistance of ProTaper Universal (PTU), ProTaper Gold (PTG), and ProTaper Next (PTN) nickel titanium (NiTi) rotary files was evaluated. Fifteen instruments of each type were selected, totaling 195 files. The instruments were rotated until fracture in an artificial canal with dimensions corresponding to the dimensions of each instrument tested: +0.1 mm in width and 0.2 mm in depth, an angle of curvature of 45°, a radius of curvature of 5 mm, and a center of curvature 5 mm from the instrument tip. The fracture surfaces of three representative samples of each subgroup were examined using scanning electron microscopy (SEM). Time to fracture was analyzed via analysis of variance and Tukey's tests ($P < 0.05$). PTG F1 and F2 had significantly higher resistance than PTU F1 and PTN X2, and PTU F2 and PTN X3, respectively. PTN X2 showed a significantly higher resistance than PTU F1. The PTG series demonstrated superior cyclic fatigue (CF) behavior compared with that of the PTU and PTN series.

Keywords: cyclic; fatigue; gold; next; ProTaper; universal

1. Introduction

Due to iatrogenic procedural errors associated with the material stiffness of stainless-steel instruments, nickel–titanium (NiTi) material was introduced in the production of endodontic files [1]. The main characteristics of NiTi rotary instruments include memory shape, superior elasticity, and a centered canal preparation. In particular, the elastic flexibility of NiTi instruments is two to three times higher than that of stainless-steel instruments due to their lower modulus of elasticity [2,3]. The material properties of NiTi and stainlessness rotary files are presented in Table 1 [4].

Despite the elastic flexibility of NiTi rotary systems, instrument fracture has been reported [5,6]. The failure of rotary NiTi files can be either flexural (cyclic) or torsional [7]. The majority of studies have shown that cyclic fatigue (CF) fracture occurs when an instrument is flexed in the maximum curvature region of the canal while rotating freely, resulting in repeated tension–compression cycles [6,8]. The tension occurs on the part of the instrument on the outside of the curve, whereas the compression occurs on the other part on the inside of the curve. Therefore, these repeated cycles, caused by the rotation of the instrument within the curved canal, result in instrument fracture due to the increase in the cyclic fatigue of the instrument over time. Torsional fatigue occurs when an instrument tip is locked in a canal, while the body continues to rotate. Therefore, fracture of the tip becomes unpreventable when the torque exerted by the handpiece exceeds the elastic limit of the metal [8]. However, one of the limitations in in vitro studies of the cyclic fatigue behavior of NiTi instruments is the difficulty of

assessing the clinical relevance of published tests results, where there are several factors, including torsional fatigue, at play at the same time.

Table 1. Properties of NiTi and stainless steel rotary files.

Properties	Ni–Ti Alloy	Stainless Steel
Ultimate tensile strength	~1240 MPa	~760 MPa
Density	6.45 gm/cm ³	8.03 gm/cm ³
Recoverable elongation	8%	0.8%
Effective modulus	~48 GPa	~193 GPa
Coefficient of thermal expansion	$6.6 \times 10^{-6} - 11 \times 10^{-6} \text{ } ^\circ\text{C}^{-1}$	$17.3 \times 10^{-6} \text{ } ^\circ\text{C}^{-1}$
Micro-hardness	303–362 VHN	522–542 VHN

The mechanical behavior and elastic flexibility of the NiTi alloy were improved by changing the transformation behavior of the alloy through heat treatment [9]. The NiTi alloy contains three microstructural phases (austenite, martensite, and R phase). Instruments in the martensite phase can be soft, ductile, and easily deformed and can recover their shape upon heating above the transformation temperature. Compared with conventional super-elastic NiTi, which shows a finish temperature of 16–31 °C [7,9], controlled memory wire and M-wire instruments show increased austenite transformation finish temperatures of approximately 55 and 50 °C, respectively [10]. Therefore, at body temperature, the conventional super-elastic NiTi file has an austenite structure, whereas an NiTi file with thermal processing is essentially in the martensite phase [9].

ProTaper Universal (PTU) and ProTaper Gold (PTG) rotary instruments possess the same geometries; however, PTG instruments have been metallurgically enhanced through heat-treatment technology in an attempt to improve flexibility, resistance to CF, and durability [7,11]. ProTaper Next (PTN) instruments are made of M-wire, which is fabricated by the thermomechanical processing of NiTi wire blanks [5]. In addition, fracture resistance has been improved in PTN instruments due to the unique asymmetrical rotary motion and reduced contact points between the instrument and root canal walls [5].

In the endodontic literature, rotational bending is applied to test for CF in NiTi rotary instruments. Several devices and methods have been used to evaluate the in vitro CF fracture resistance of NiTi rotary endodontic instruments [8]. In addition to two important parameters used to determine the shape of the root canal, i.e., the angle and radius of curvature [6], some studies have reported that the results obtained might be unreliable and inconsistent if the established device parameters do not follow each instrument's morphologic and geometric features [8]. To overcome this problem, multiple devices with artificial canals that have dimensions that exceed those of the tested instruments by 0.1–0.3 mm have been used [12–14].

No previous study has compared the CF resistance of all the ProTaper instruments among the three different generations. Therefore, the aim of the present study was to assess the CF behavior of the PTU, PTG, and PTN NiTi rotary files.

2. Materials and Methods

2.1. Preparation of Artificial Canals

The laser micromachining technique was used to machine artificial canals in stainless-steel plates with dimensions of 100 mm × 50 mm × 10 mm. Machining was performed using the LASERTEC 40 (Deckel Maho Gildemeister, Hamburg, Germany), which consists of a Q-switched Neodymium-doped Yttrium Aluminum Garnet (Nd: Y3Al5O12 (Nd: YAG)) laser operating at a wavelength of 1064 nm with a maximum average power of 30 W.

The artificial canal to be machined was modeled using CATIA V5[®] software (Dassault Systèmes, Version 5, Vélizy, France), and laser path programming was performed with a Standard Triangle

Language file of the proprietary machine software. After the laser process parameters were established, the laser was focused on the workpiece with the aid of a galvano scanner, and the canal was then machined layer by layer [15].

The artificial canals were machined in stainless-steel blocks with dimensions corresponding to the dimensions of the instrument tested: +0.1 mm in width and +0.2 mm in depth, with an angle of curvature of 45° , a radius of curvature of 5 mm, and a center of curvature 5 mm from the tip of the instrument [6,8] (Figure 1).

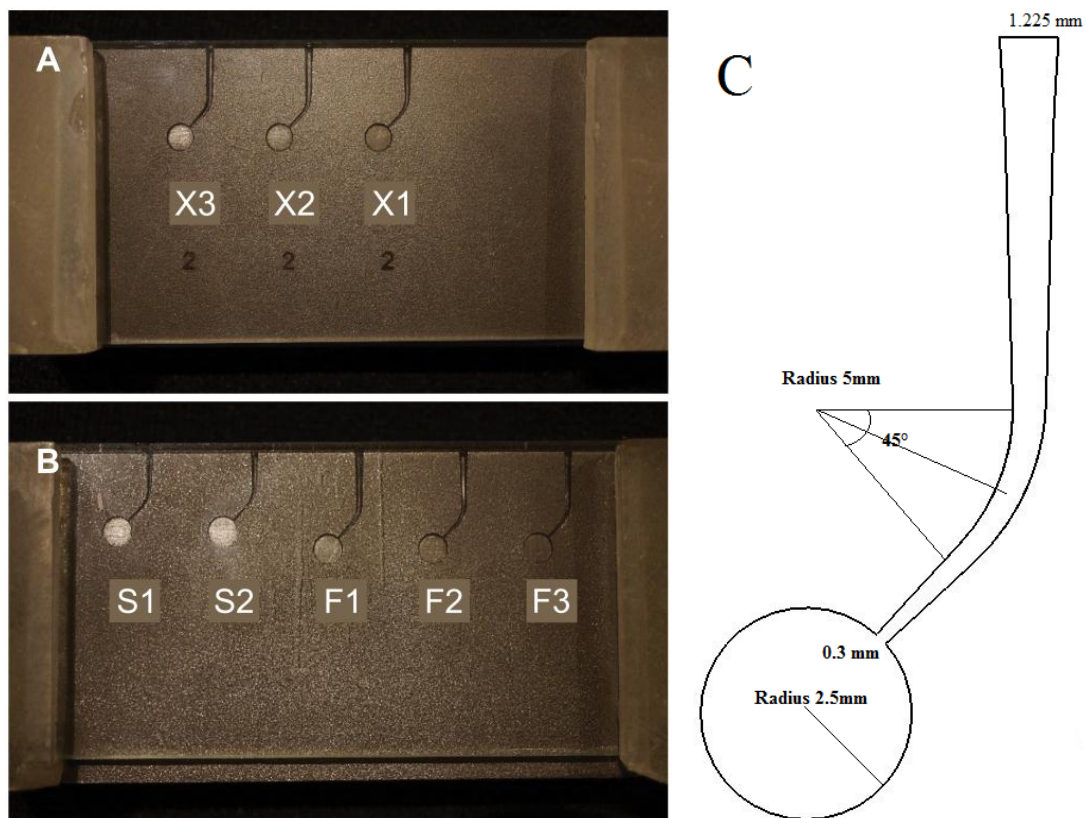


Figure 1. Custom-made stainless-steel blocks with dimensions corresponding to the dimensions of ProTaper Next (PTN) (A), ProTaper Gold (PTG), and ProTaper Universal (PTU) (B): +0.1 mm in width and +0.2 mm in depth, with an angle of curvature of 45° , a radius of curvature of 5 mm, and a center of curvature 5 mm from the tip of the instrument. (C) Two-dimensional draft of artificial canal for PTU F1 instrument.

The dimensions of the PTU and PTG instruments were recorded according to the manufacturer as shown in Table 2. The actual dimension for the PTN from the manufacturer along with the maximum diameters of the PTN instruments measured using Digimizer[®] software (MedCalc Software, version 4.5., Ostend, Belgium) are shown in Table 3.

Table 2. Dimensions of PTU and PTG from the manufacturer.

Active Part Length (mm)	Diameter (mm)				
	S1	S2	F1	F2	F3
0	0.170	0.200	0.200	0.250	0.300
1	0.190	0.240	0.270	0.330	0.390
2	0.220	0.285	0.340	0.410	0.480
3	0.260	0.335	0.410	0.490	0.570
4	0.305	0.390	0.465	0.550	0.640
5	0.355	0.450	0.520	0.610	0.710
6	0.415	0.510	0.575	0.665	0.760
7	0.485	0.570	0.630	0.720	0.810
8	0.565	0.630	0.685	0.775	0.860
9	0.655	0.690	0.740	0.830	0.910
10	0.755	0.760	0.795	0.885	0.960
11	0.855	0.850	0.850	0.940	1.010
12	0.960	0.955	0.905	0.995	1.060
13	1.075	1.070	0.960	1.050	1.110
14	1.185	1.185	1.015	1.105	1.160
15			1.070	1.160	1.210
16			1.125	1.215	1.260

Table 3. Dimensions of the PTN from the manufacturer.

Active Part Length (mm)	Diameter (mm)					
	X1		X2		X3	
	Actual	Maximum	Actual	Maximum	Actual	Maximum
16	1.16	1.26	1.2	1.3	1.2	1.34
13	0.98	1.06	1.11	1.15	1.09	1.14
9	0.7	0.76	0.84	1.06	0.89	1
6	0.49	0.534	0.63	0.7	0.71	0.78
3	0.31	0.35	0.43	0.45	0.53	0.65
1	0.21	0.23	0.31	0.34	0.38	0.52
0	0.17	0.17	0.25	0.25	0.3	0.3

2.2. Cyclic Fatigue Testing

Fifteen rotary instruments of each type (PTU S1, S2, F1, F2, and F3, PTG S1, S2, F1, F2 and F3, and PTN X1, X2, and X3), totaling 195 instruments of 25 mm in length, were used in this study.

Stainless-steel blocks were attached to a main frame to which a mobile support for the handpiece was connected. The dental handpiece was mounted on a mobile device that allowed for the simple placement of each instrument inside the artificial canal as shown in Figure 2. To prevent the instruments from slipping out and to allow for observation of the instruments, the artificial canals were covered with glass.

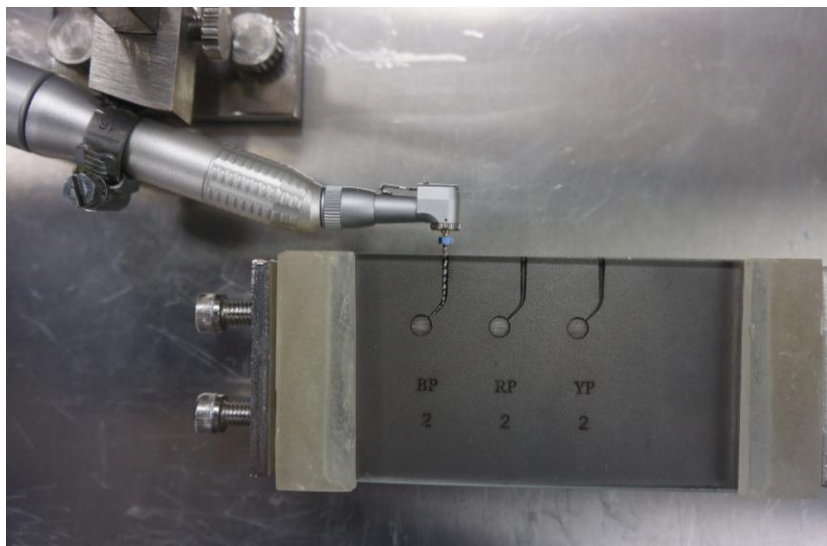


Figure 2. CF testing device illustrating positioning of dental handpiece, NiTi rotary instrument, and stainless steel block.

A pilot study was conducted to confirm the reliability of the CF device. All of the instruments were rotated at the speed recommended by the manufacturer (300 rpm) until fracture. The artificial canals were lubricated with synthetic oil (3-In-One Multi-Purpose Oil, WD-40[®], San Diego, CA, USA) to reduce the friction of the tested file against the artificial canal walls. The motor and timer were then simultaneously activated. During each test, the instrument was monitored and visualized through the glass until fracture occurred, and the time to fracture was registered in seconds. Figure 3 shows the rotary files before and after fracture. The fractured surface was examined using SEM (JEOL 6360LV Scanning Electron Microscope, Tokyo, Japan) after preparation with $\geq 99.8\%$ ethanol.

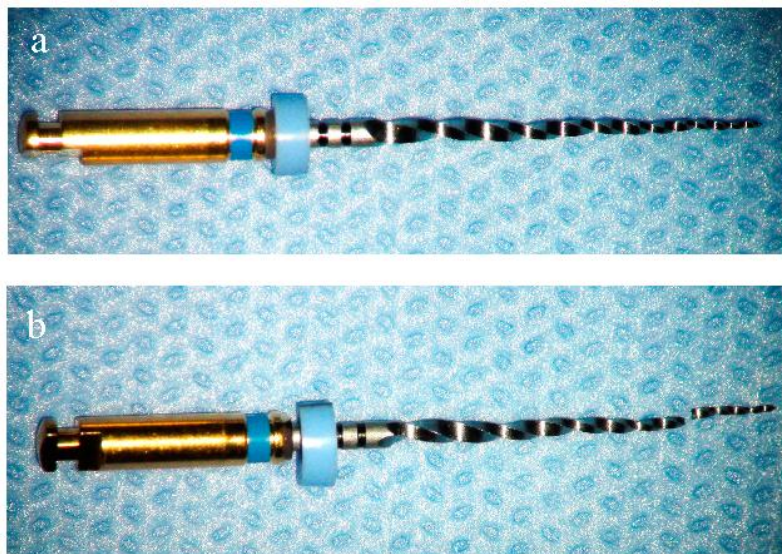


Figure 3. ProTaper Next X3 before (a) and after (b) fracture.

Statistical analysis of the empirical data is essential for the proper interpretation and prediction of results. There are many statistical methods such as analysis of variance (ANOVA), regression analysis, and correlation for analyzing data and representation of results [16]. Reports are available on the use of statistical methods for cyclic fatigue failure analysis [17] and fatigue life prediction [18].

In this work, one-way ANOVA and Tukey’s tests were performed to analyze and compare the means. Statistical significance was set at $P < 0.05$. Weibull reliability analysis was performed and the probability of survival was calculated for the tested instruments.

3. Results

The mean times to fracture and standard deviations for the PTU, PTG, and PTN instruments are presented in Table 4. The CF behaviors of the PTU, PTG, and PTN series are presented in Figure 4. Comparing the instruments with similar $D5 \pm 0.01$ mm, one-way ANOVA and Tukey’s post-hoc tests showed that PTG F1 and F2 had significantly higher CF resistance than PTU F1 and PTN X2, and PTU F2 and PTN X3, respectively. PTN X2 showed a significantly higher CF resistance than PTU F1. However, there was no significant difference between PTU F2 and PTN X3 in terms of CF resistance.

Table 4. Instrument type, sample size, time to fracture (seconds; mean \pm SD), and Weibull calculations.

Instrument	N	Mean \pm SD	Weibull Modulus	R-Squared	Predicted Time in Seconds for 99% Survival
PTU					
S1	15	166.07 \pm 34.3	4.809	0.914	69
S2	15	170.40 \pm 21.9	8.500	0.924	104
F1	15	101.47 \pm 13.6	8.528	0.986	62
F2	15	93.20 \pm 15.2	6.405	0.965	48
F3	15	87.20 \pm 13.8	6.338	0.918	44
PTG					
S1	15	352.5 \pm 57.4	6.357	0.916	181
S2	15	294.0 \pm 34.2	5.495	0.839	135
F1	15	239.40 \pm 25.4	9.276	0.952	152
F2	15	198.40 \pm 14.6	13.415	0.951	145
F3	15	183.40 \pm 16.6	10.352	0.872	122
PTN					
X1	15	334.69 \pm 67.5	5.062	0.865	154
X2	15	176.93 \pm 32.3	5.221	0.950	78
X3	15	133.27 \pm 31.5	4.274	0.781	49

SD: standard deviation. Weibull calculations included the Weibull modulus (m), the coefficient of determination (R-squared), and the predicted time in seconds for 99% survivability.

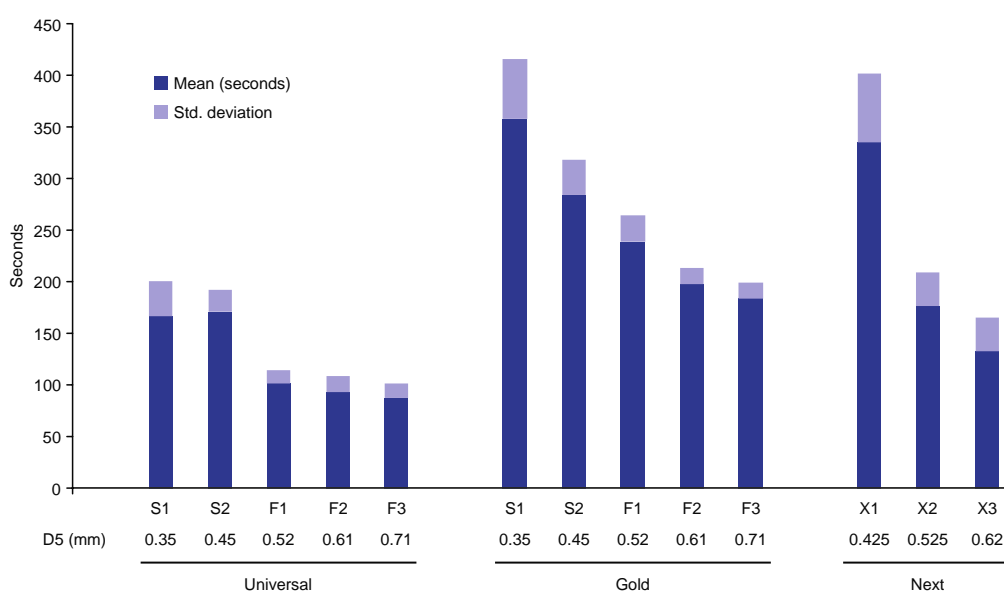


Figure 4. The mean time to fracture (s), standard deviation (SD) and D5 (mm) for PTU, PTG, and PTN.

Probabilistic modeling of fatigue failure and reliability assessment has been done for various engineering components such as turbine blades [19], turbine disc [20], and railway axles [21], which are subjected to variable loading conditions. Reliability analysis is important for the establishment of suitable safety levels for any device or system.

Weibull reliability analysis results and the probabilities of survival calculated for the PTU, PTG, and PTN instruments are presented in Table 4. The PTG series showed higher reliability than the PTU and PTN series. PTG S1 showed the longest resistance, with 181 s at 99% survival. Regarding the instruments with similar diameters at 5 mm from the tip, rotation for 152 s was predicted for PTG F1 at 99% reliability compared with 78 and 62 s for PTN X2 and PTU F1, respectively. Additionally, rotation for 145 s was predicted for PTG F2 at 99% reliability compared with 49 and 48 s for PTN X3 and PTU F2, respectively.

Figure 5 shows the fractography analysis of the PTU S1 sample. Two distinct regions were noticed: one with fatigue striations (Region a) and another with a dimpled surface (Region b) (Figure 5A). The crack initiates at the edge and propagates to the fatigue striations (Figure 5B). Micro-voids produced coalesce with each other and weakens the material (Figure 5C), after which ductile fracture occurs, which is evident from the dimpled surface in Figure 5D, until failure. The round dimples indicate normal rupture caused by tensile stresses.

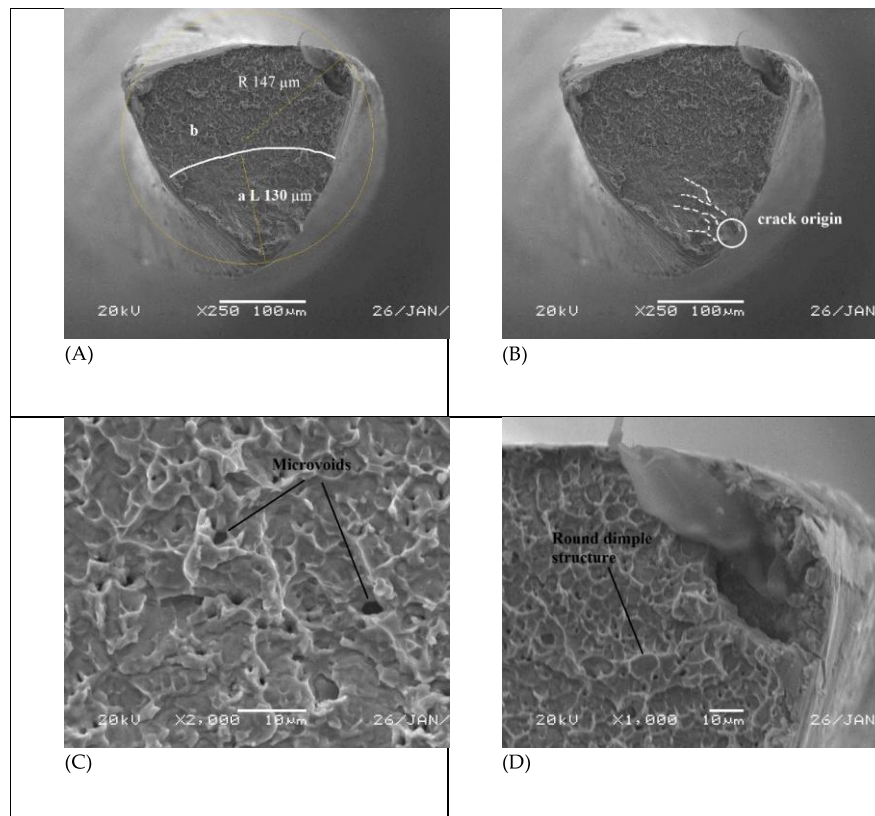


Figure 5. SEM analysis of PTU S1 sample. (A) Overall cross-sectional view (B) Crack initiation (C) micro-voids. (D) Dimpled structures.

4. Discussion

In this study, the tested instruments were selected because they shared the same recommended scheme of instrumentation. Generally, compared with the PTU and PTN series, the PTG series in this study demonstrated favorable CF behavior. However, the PTU, PTG, and PTN instruments vary in their tapering schemes, cross sections, axes of rotations, and alterations in metallurgic processing. Therefore, comparisons were performed among instruments of similar diameter (± 0.01 mm) at the center of the

curvature to minimize confounding factors. The PTG instruments were most resistant to CF, followed by PTN and PTU. However, the difference between PTN X3 and PTU F2 was not significant.

The higher CF resistance of the PTG and PTN instruments can be attributed to the thermomechanical treatment of these instruments [9]. Furthermore, instrument morphology is considered a significant determinant of CF behavior and can explain the greater CF resistance of the PTG instruments compared with that of the PTN instruments. Some studies have shown that instrument design is not an important determinant of CF resistance [22,23], whereas others have suggested that a different cross-sectional design is a main determinant of the CF resistance of different files [10,12,14,24,25]. Cheung et al. reported that instruments with a triangular cross-section demonstrated a higher fatigue resistance than those with a square cross section [26].

Yong et al. reported a favorable balanced relationship of flexibility, peak torque, and cyclic fatigue resistance of NiTi rotary instruments when compared to stainless steel instruments [27]. Furthermore, the thermomechanically treated NiTi instruments demonstrated greater flexibility and fatigue resistance than conventional SE NiTi instruments of similar diameter and geometry.

Several studies have compared the CF resistance of different NiTi rotary systems. Hieawy et al. tested the CF resistance of PTG and PTU instruments of sizes S1 to F3 using a 3-point bending device at a curvature of 40° with a 6 mm radius [7]. Their results showed that the PTG file had a significantly higher CF resistance than did the PTU file ($P < 0.001$). In addition, the S1 and S2 files were more resistant to fatigue failure than the F1 to F3 files in both the PTG and PTU systems ($P < 0.001$). PTG S1 showed the highest CF resistance among all files ($P < 0.001$), whereas PTU F3 showed the lowest CF resistance. These findings agree with the results from the PTU and PTG series in this study.

Perez-Higueras et al. reported that PTN X2 and X3 were more resistant than were PTU F1 and F2, respectively, when tested in stainless-steel curved canals at a curvature of 60° with a 3 mm radius [28]. Nguyen et al. compared the CF among PTU and PTN instruments with a curvature of 90° and a 5 mm radius. Their results indicated that PTU F1/F2 had a higher CF resistance than PTN X2/X3, respectively; however, this difference was not significant [29].

Weibull analysis can predict a product's resistance and be used to compare the reliability of various product designs. Nguyen et al. discussed in detail the clinical relevance and the advantages of Weibull analysis in such cases when they compared CF with PTN, PTU, and Vortex Blue rotary instruments [29]. Weibull prediction can also provide the clinician with information about the time required for a rotating instrument in a canal to fracture.

Topographic features of the fracture surfaces of all broken instruments were analyzed using SEM. The findings of this study are in agreement with previous studies where the fracture surfaces of all groups showed typical features of CF with one or more crack initiation areas, fatigue striation, and a fast fracture zone with dimples [5,7].

The KT (Kitagawa–Takahashi) diagram represents the boundary in terms of crack size and stress range for infinite fatigue life [30]. The present work can be extended to define the KT diagram for fatigue life prediction based on various approaches such as the probabilistic S-N model, EIFS (equivalent initial flaw size), and fatigue crack growth models [18,31,32]. The experimental fatigue life data can then be plotted and compared with the KT diagram.

5. Conclusions

Compared with the PTU and PTN series, the PTG series demonstrated superior CF behavior. The PTU series was the least resistant to CF. As fatigue resistance is one of the most common factors attributed to instrument fracture and considering the recent advances in technology, international standards for CF testing devices should be established to minimize the variations in reported data. Furthermore, the experimental results and SEM analysis used in this work can be used to define the KT diagram for fatigue life prediction.

Acknowledgments: The authors thank King Saud University, College of Dentistry Research Center (CDRC), particularly the physical laboratory staff, for their assistance in conducting this study.

Author Contributions: Abdullah Alqedairi and Hussam Alfawaz designed the study, supervised and performed the experiments, analyzed the data, and finalized the manuscript. Amani bin Rabba, Areej Almutairi, and Sarah Alnafaiy performed the experiments and wrote the initial draft of manuscript. Muneer Khan Mohammed designed and fabricated the artificial canals, helped in statistical analysis and wrote the laser micromachining part of the manuscript.

Conflicts of Interest: The authors have no conflicts of interest to declare.

References

1. Walia, H.; Brantley, W.A.; Gerstein, H. An initial investigation of the bending and torsional properties of nitinol root canal files. *J. Endod.* **1988**, *14*, 346–351. [[CrossRef](#)]
2. Hülsmann, M.; Peters, O.A.; Dummer, P.M.H. Mechanical preparation of root canals: Shaping goals, techniques and means. *Endod. Top.* **2005**, *10*, 30–76. [[CrossRef](#)]
3. Peters, O.A. Current challenges and concepts in the preparation of root canal systems: A review. *J. Endod.* **2004**, *30*, 559–567. [[CrossRef](#)] [[PubMed](#)]
4. Nitinol and Stainless Steel: Property Comparison. Available online: <http://jmmedical.com/resources/231/Comparison-of-Properties-of-NiTi-and-Stainless-Steel.html> (accessed on 28 December 2017).
5. Elnaghy, A.M.; Elsaka, S.E. Assessment of the mechanical properties of protaper next nickel-titanium rotary files. *J. Endod.* **2014**, *40*, 1830–1834. [[CrossRef](#)] [[PubMed](#)]
6. Pruett, J.P.; Clement, D.J.; Carnes, D.L., Jr. Cyclic fatigue testing of nickel-titanium endodontic instruments. *J. Endod.* **1997**, *23*, 77–85. [[CrossRef](#)]
7. Hieawy, A.; Haapasalo, M.; Zhou, H.; Wang, Z.J.; Shen, Y. Phase transformation behavior and resistance to bending and cyclic fatigue of protaper gold and protaper universal instruments. *J. Endod.* **2015**, *41*, 1134–1138. [[CrossRef](#)] [[PubMed](#)]
8. Plotino, G.; Grande, N.M.; Cordaro, M.; Testarelli, L.; Gambarini, G. A review of cyclic fatigue testing of nickel-titanium rotary instruments. *J. Endod.* **2009**, *35*, 1469–1476. [[CrossRef](#)] [[PubMed](#)]
9. Shen, Y.; Zhou, H.M.; Zheng, Y.F.; Peng, B.; Haapasalo, M. Current challenges and concepts of the thermomechanical treatment of nickel-titanium instruments. *J. Endod.* **2013**, *39*, 163–172. [[CrossRef](#)] [[PubMed](#)]
10. Haikel, Y.; Serfaty, R.; Bateman, G.; Senger, B.; Allemann, C. Dynamic and cyclic fatigue of engine-driven rotary nickel-titanium endodontic instruments. *J. Endod.* **1999**, *25*, 434–440. [[CrossRef](#)]
11. Ruddle, C.J.; Machtou, P.; West, J.D. Endodontic canal preparation: Innovations in glide path management and shaping canals. *Dent. Today* **2014**, *33*, 118–123. [[PubMed](#)]
12. Plotino, G.; Grande, N.M.; Sorci, E.; Malagnino, V.A.; Somma, F. A comparison of cyclic fatigue between used and new mtwo Ni-Ti rotary instruments. *Int. Endod. J.* **2006**, *39*, 716–723. [[CrossRef](#)] [[PubMed](#)]
13. Plotino, G.; Grande, N.M.; Sorci, E.; Malagnino, V.A.; Somma, F. Influence of a brushing working motion on the fatigue life of NiTi rotary instruments. *Int. Endod. J.* **2007**, *40*, 45–51. [[CrossRef](#)] [[PubMed](#)]
14. Gambarini, G.; Grande, N.M.; Plotino, G.; Somma, F.; Garala, M.; De Luca, M.; Testarelli, L. Fatigue resistance of engine-driven rotary nickel-titanium instruments produced by new manufacturing methods. *J. Endod.* **2008**, *34*, 1003–1005. [[CrossRef](#)] [[PubMed](#)]
15. Mohammed, M.K.; Al-Ahmari, A.; Umer, U. Multiobjective optimization of Nd: YAG direct laser writing of microchannels for microfluidic applications. *Int. J. Adv. Manuf. Technol.* **2015**, *81*, 1363–1377. [[CrossRef](#)]
16. Montgomery, D.C. *Design and Analysis of Experiments*; John Wiley & Sons: New York, NY, USA, 2017; ISBN 978-1-119-11347-8.
17. De Oliveira Correia, J.A.F.; Pedrosa, B.A.S.; Raposo, P.C.; De Jesus, A.M.P.; dos Santos Gervásio, H.M.; Lesiuk, G.S.; da Silva Rebelo, C.A.; Calçada, R.A.B.; da Silva, L.A.P.S. Fatigue Strength Evaluation of Resin-Injected Bolted Connections Using Statistical Analysis. *Engineering* **2017**. [[CrossRef](#)]
18. Correia, J.A.F.O.; Blason, S.; De Jesus, A.M.P.; Canteli, A.F.; Moreira, P.M.G.P.; Tavares, P.J. Fatigue life prediction based on an equivalent initial flaw size approach and a new normalized fatigue crack growth model. *Eng. Fail. Anal.* **2016**, *69*, 15–28. [[CrossRef](#)]
19. Zhu, S.-P.; Huang, H.-Z.; Peng, W.; Wang, H.-K.; Mahadevan, S. Probabilistic Physics of Failure-based framework for fatigue life prediction of aircraft gas turbine discs under uncertainty. *Reliab. Eng. Syst. Saf.* **2016**, *146*, 1–12. [[CrossRef](#)]

20. Zhu, S.P.; Liu, Q.; Lei, Q.; Wang, Q. Probabilistic fatigue life prediction and reliability assessment of a high pressure turbine disc considering load variations. *Int. J. Damage Mech.* **2017**, 1056789517737132. [[CrossRef](#)]
21. Zhu, S.P.; Huang, H.Z.; Li, Y.; Liu, Y.; Yang, Y. Probabilistic modeling of damage accumulation for time-dependent fatigue reliability analysis of railway axle steels. *Proc. Inst. Mech. Eng. Part F J. Rail Rapid Transit* **2015**, 229, 23–33. [[CrossRef](#)]
22. De Melo, M.C.C.; de Azevedo Bahia, M.G.; Buono, V.T.L. Fatigue resistance of engine-driven rotary nickel-titanium endodontic instruments. *J. Endod.* **2002**, 28, 765–769.
23. Cheung, G.S.; Darvell, B.W. Low-cycle fatigue of NiTi rotary instruments of various cross-sectional shapes. *Int. Endod. J.* **2007**, 40, 626–632. [[CrossRef](#)] [[PubMed](#)]
24. Ray, J.J.; Kirkpatrick, T.C.; Rutledge, R.E. Cyclic fatigue of endosequence and K3 rotary files in a dynamic model. *J. Endod.* **2007**, 33, 1469–1472. [[CrossRef](#)] [[PubMed](#)]
25. Tripi, T.R.; Bonaccorso, A.; Condorelli, G.G. Cyclic fatigue of different nickel-titanium endodontic rotary instruments. *Oral Surg. Oral Med. Oral Pathol. Oral Radiol. Endod* **2006**, 102, e106–e114. [[CrossRef](#)] [[PubMed](#)]
26. Cheung, G.S.; Zhang, E.W.; Zheng, Y.F. A numerical method for predicting the bending fatigue life of NiTi and stainless steel root canal instruments. *Int. Endod. J.* **2011**, 44, 357–361. [[CrossRef](#)] [[PubMed](#)]
27. Gao, Y.; Gutmann, J.L.; Wilkinson, K.; Maxwell, R.; Ammon, D. Evaluation of the impact of raw materials on the fatigue and mechanical properties of profile vortex rotary instruments. *J. Endod.* **2012**, 38, 398–401. [[CrossRef](#)] [[PubMed](#)]
28. Perez-Higueras, J.J.; Arias, A.; de la Macorra, J.C.; Peters, O.A. Differences in cyclic fatigue resistance between protaper next and protaper universal instruments at different levels. *J. Endod.* **2014**, 40, 1477–1481. [[CrossRef](#)] [[PubMed](#)]
29. Nguyen, H.H.; Fong, H.; Paranjpe, A.; Flake, N.M.; Johnson, J.D.; Peters, O.A. Evaluation of the resistance to cyclic fatigue among protaper next, protaper universal, and vortex blue rotary instruments. *J. Endod.* **2014**, 40, 1190–1193. [[CrossRef](#)] [[PubMed](#)]
30. Kitagawa, H.; Takahashi, S. Applicability of Fracture Mechanics to Very Small Cracks or the Cracks in the Early Stages. In Proceedings of the Second International Conference on Mechanical Behavior of Materials, American Society for Metals, Metals Park, OH, USA, 16–20 August 1976; p. 627.
31. Correia, J.; De Jesus, A.; Fernández-Canteli, A.; Brighenti, R.; Moreira, P.; Calçada, R. A procedure to obtain the probabilistic kitagawa-takahashi diagram. *UPB Sci. Bull. Ser. Mech. Eng.* **2016**, 78, 3–12.
32. Maierhofer, J.; Gänser, H.-P.; Pippan, R. Modified Kitagawa–Takahashi diagram accounting for finite notch depths. *Int. J. Fatigue* **2015**, 70, 503–509. [[CrossRef](#)]



© 2018 by the authors. Licensee MDPI, Basel, Switzerland. This article is an open access article distributed under the terms and conditions of the Creative Commons Attribution (CC BY) license (<http://creativecommons.org/licenses/by/4.0/>).